ISSN 1009 - 3095 *Journal of Zhejiang University(SCIENCE)* V.2, No.2, P.121 - 127, Apr. - June, 2001
http://www.chinainfo.gov.cn/periodical; http://www.zju.edu.cn;
http://lib.zju.edu.cn/English; http://www.zjupress.com

MICROSTRUCTURE OF AS-MELT SPUN Al-Cu-Mg-Fe-Ni ALLOY AND ITS VARIATION IN CONTINUOUS HEAT TREATMENT

YAN Mi (严 密), LUO Wei (罗 伟), WU Zhen-tai(邬震泰)

(*Dept. of Mater. Sci. and Eng., Zhejiang University, Hangzhou 310027, China*)

Received June 1, 2000; revision accepted Sept.21, 2000

Abstract: A commercial AA2618 alloy was treated through melt spinning at rotating speeds of 20 and 40 $m \cdot s^{-1}$. The as-melt spun ribbons were characterized by a combination of optical microscopy (OPM), scanning electron microscopy (SEM), transmission electron microscopy (TEM) and X-ray diffraction (XRD). The microstructural evolution of the ribbons in a continuous heating process was investigated, and the microhardness was also measured under different conditions. It was found that Al_xFeNi is prone to precipitate in AA2618 alloy due to the minimal solubility of iron and nickel. Fine Al_xFeNi particles appeared along the grain boundaries at the chilling sides of as-melt spun ribbons, and at both the grain boundaries and in the interior of grains at the free sides. On continuous heating Al_xFeNi precipitated steadily and uniformly throughout the matrix until melting. The microhardness of as-melt spun ribbons decreased significantly from the chilling surfaces to free surfaces. Precipitation of Al_xFeNi lowered the hardness of the alloy.

Key words: melt spinning, AA2618, ribbon, microstructure
Document code: A **CLC number:** TG146.2+1

INTRODUCTION

There are reports of extensive investigations on the precipitation and ageing hardening of Al-Cu-Mg alloys (Chen et al., 1997; Shih et al., 1996; Huang et al., 1995). Copper and magnesium contribute to the precipitation hardening at temperatures of up to 200 ℃. Additions of iron and nickel to Al-Cu-Mg alloys lead to improved mechanical properties at high temperatures of up to 238 ℃ (Gomes et al., 1996; Zhou et al., 1991). The effects of increasing addition of iron and nickel in Al-Cu-Mg alloys intended for service at even higher temperatures is now being considered (Zhang et al., 1991). However, understanding of the effect of iron and nickel in the Al-Cu-Mg alloys is still very limited.

AA2618 is an Al-Cu-Mg-Fe-Ni alloy, primarily applied for production of pistons and aircraft engine components for operation at elevated temperatures (Oguocha et al., 1996). The formation of Al_xFeNi in the alloy under different processing conditions (Zhang et al., 1991; Oguocha et al., 1996; Yao et al., 1996) had been proved, although the structure of the aluminide is still not recognized completely. The aluminide was determined (Zhang et al., 1991; Oguocha et al., 1996; Yao et al., 1996). As Al_9FeNi, having a primitive monoclinic structure with lattice parameters $a = 0.6213$ nm, $b = 0.6290$ nm, $c = 0.8557$ nm and $\beta = 94.76°$. In Oguocha et al.'s work (1996), the structural formula of different aluminide particles in cast AA2618 was found to be different, depending on the aluminum content in it; so the aluminide was characterized as Al_xFeNi, having a C-centered monoclinic structure with lattice parameters $a = 0.8673$ nm, $b = 0.9000$ nm, $c = 0.8591$ nm, $\beta = 83.504°$. No matter what structure the aluminide has, Al_xFeNi was shown to have significant effects on the mechanical performance of AA2618. The main objective of this work is to gain understanding of the forming conditions of Al_xFeNi as well as its effect on the hardening of AA2618 alloy subjected to rapid solidification processing through melt spinning. In addition to observing the microstructural features of AA2618 alloy after melt spinning, primary attention is on the precipitation of Al_xFeNi and its morphology evolution in the subsequent heat processing. The structure of Al_xFeNi is not within the scope of this investigation, since different processing routes and heat treatment history should be responsible for the difference in the reported aluminide structure.

* Project supported by Special Research Foundation of High-Education Ph.D. Subjects, Education Ministry of P. R. China.

EXPERIMENTAL DETAILS

The nominal composition of AA2618 is presented in Table 1. In the attempt to eliminate Al_xFeNi in the alloy matrix, about 5 grams alloy strips cut from the as-supplied commercial alloy were cleaned in methanol, and loaded into a quartz tube. The strips were remelted at 800 ℃ in argon, and then ejected from an orifice at the tube bottom to the surface of a copper drum. The quartz tube orifice diameter was 0.83 mm. The thicknesses of the ribbons were 50 – 70 μm and 40 – 50 μm when the tangential rotation speed of the copper drum was 20 and 40 $m \cdot s^{-1}$ respectively.

Table 1 The elemental composition of commercial AA2618 alloy (%)

Cu	Mg	Fe	Ni	Si	Ti	Al
2.3	1.6	1.1	1.0	0.18	0.07	bal

The as-melt spun ribbons were then subjected to microstructural characterization by a combination of OPM, SEM, TEM, EDX and XRD. To observe different microstructural features across the ribbon, the ribbon was polished either at the chilling surface (in contact with the copper drum), or at the free surface (in contact with the atmosphere) in the preparation of TEM foils, then further thinned by ion beam milling.

To investigate the evolution of Al_xFeNi morphology in the matrix, the ribbons were sealed in vacuumed silica tubes continuously heated at a heating rate of 5 ℃·min^{-1} to different temperatures, quenched in water. Then the ribbons were taken out and subjected to microstructural characterization. A Dupont 2000 thermal analyzer was also used to help examination of the precipitation behaviors of the ribbons. DSC tests were carried out from 150 ℃ to 750 ℃ at 5 ℃·min^{-1} heating rate under a dynamic argon atmosphere. The outputs were recorded as functions of temperature.

Measurements of microhardness were conducted at the transverse cross-sections of mounted ribbons, as a function of distance from the chilling surfaces. Microhardness was also measured on the chilling surfaces of ribbons quenched from different temperatures, as an indicator of the effects of precipitated aluminide on the strength of the alloy. Each datum was the mean value of at least 10 points, up to 50 points.

RESULTS

1. The as-melt spun structure

The thicknesses of the ribbons were 50 – 70 μm and 40 – 50 μm, at the rotating speeds of 20 and 40 $m \cdot s^{-1}$ respectively. Morphologies of both ribbons at the transverse cross-sections are respectively presented in Fig. 1 a and b. There were featureless layers adjacent to the chilling surfaces, and the structure became coarser close to the free surfaces. This layered ribbon structure was expected, and had been reported in many investigations (Rieker et al., 1991; Jones et al., 1969; Birol et al., 1996). The forming of featureless layers at the chilling sides of both ribbons may be attributed to the homogeneous nucleation.

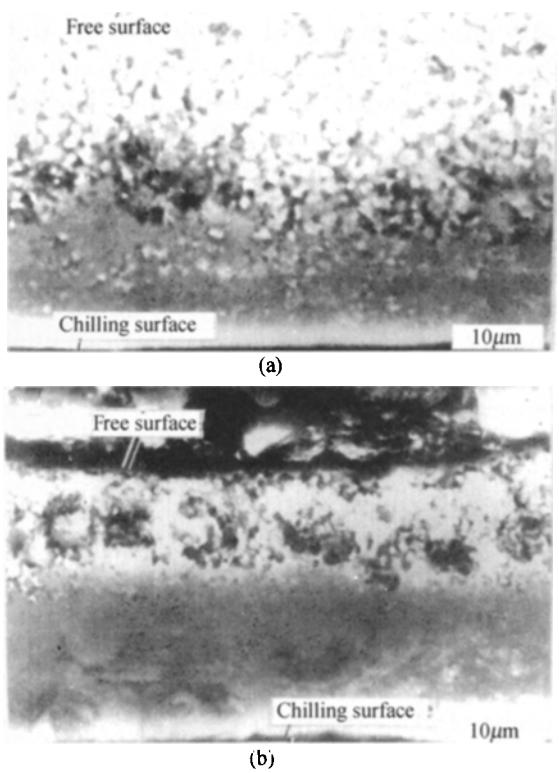

Fig. 1 Morphologies of the ribbons at the transverse cross-sections. The chilling surface is at the bottom of each micrograph
(a) at the rotation speed 20 $m \cdot s^{-1}$;
(b) at the rotation speed 40 $m \cdot s^{-1}$

XRD profiles of the 20 and 40 $m \cdot s^{-1}$ ribbons are given in Fig.2 for comparison with those of

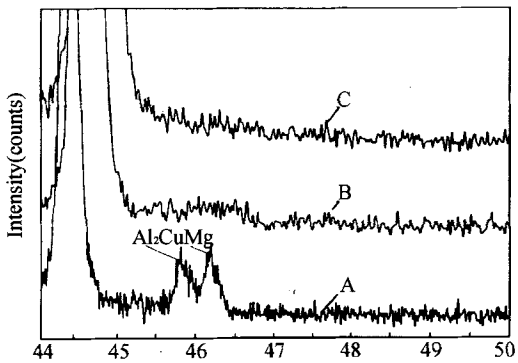

Fig.2 XRD profiles of ribbons in comparison with that of untreated AA2618 alloy: A. the untreated alloy; B. the 20 $m \cdot s^{-1}$ ribbon; C. the 40 $m \cdot s^{-1}$ ribbon

untreated commercial AA2618 alloy. The profile of the untreated alloy is labeled as A, and profiles of the 20 and 40 $m \cdot s^{-1}$ ribbons were labeled as B and C respectively. In all profiles there were no diffraction peaks that could be connected with the presence of Al_xFeNi. Profile A has clear Al_2CuMg peaks, absence of which in both ribbon profiles B and C suggests significant decreases of Al_2CuMg contents, if any, in the ribbons. Resulted from oversaturation of solute elements in the aluminum matrix, aluminum peaks shifted to higher 2θ angles in profiles B and C.

At the chilling sides, the matrix of both 20 and 40 $m \cdot s^{-1}$ ribbons was comprised of non-dendritic equiaxial grains, as shown in Fig.3a and b. The diameter of the grains was typically 0.5 μm for the 20 $m \cdot s^{-1}$ ribbon (Fig.3a), and 0.4 μm for the 40 $m \cdot s^{-1}$ ribbon (Fig.3b). As can be seen in Fig.3a, fine particles were present at the grain boundaries of the chilling side of the 20 $m \cdot s^{-1}$ ribbon (Fig.3a), the diameter of which was approximately 50 nm. Compared to the 20 $m \cdot s^{-1}$ ribbon, the grain boundaries at the chilling side of the 40 $m \cdot s^{-1}$ ribbon were relatively "clean". Precipitates were significantly fewer, but could still be found (Fig.3b). At the chilling sides of both ribbons, no precipitates could be observed in the interior of the grains.

Near the free sides, however, particles were observed to be separated out both in the interior of grains and at the grain boundaries. Moreover, grain boundaries were no longer straight (Fig.3 c and d), indicating that the growth of grains turned out to be cellular.

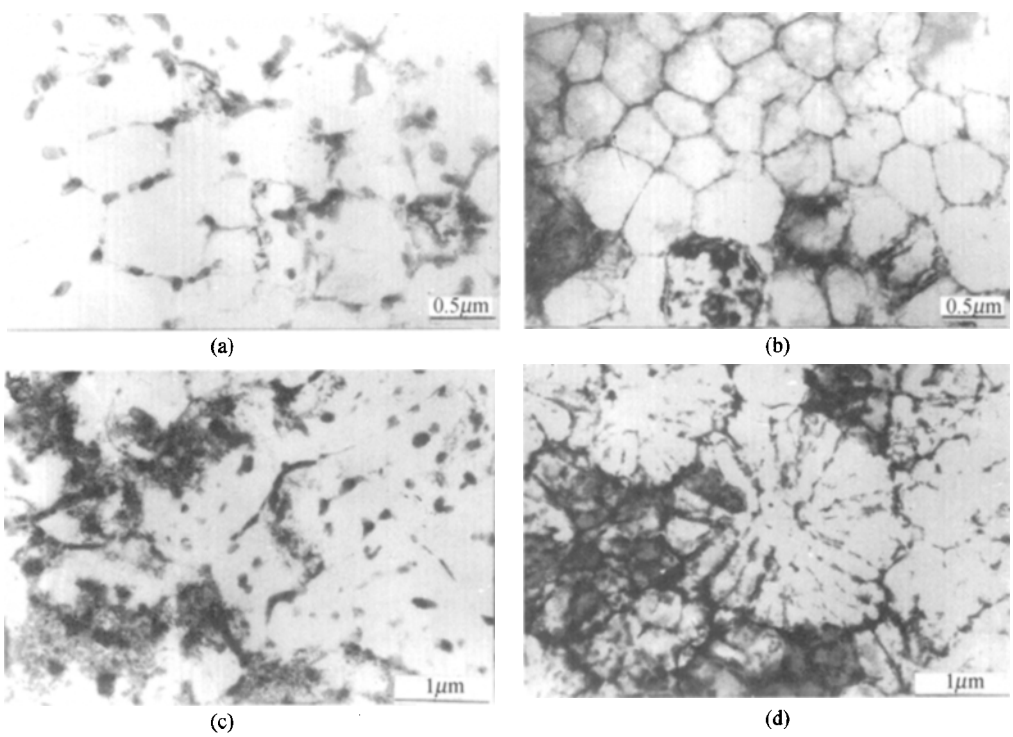

Fig.3 TEM observations at both sides of ribbons:
(a) at the chilling side of 20 $m \cdot s^{-1}$ ribbon; (b) at the chilling side of 40 $m \cdot s^{-1}$ ribbon; (c) at the free side of 20 $m \cdot s^{-1}$ ribbon; (d) rosette-like grains at the free side of 40 $m \cdot s^{-1}$ ribbon

The EDX spectrum of the particles indicated that the precipitates were not Al_2CuMg, but Al_xFeNi. The spectrum was similar to the EDX spectrum of Al_xFeNi in AA2618 given by Oguocha et al. (1996), indicating they were the same type of aluminide. A typical EDX spectrum of the precipitates is shown in Fig. 4.

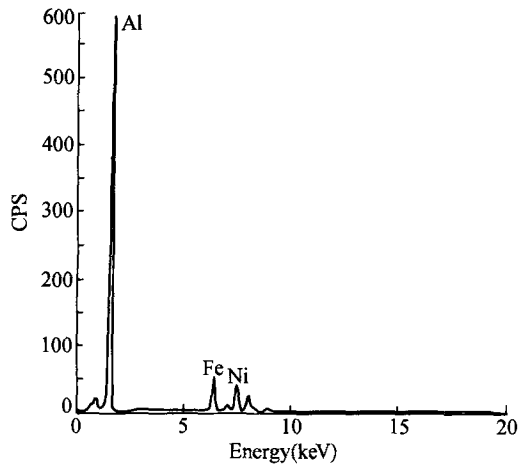

Fig. 4 A typical EDX spectrum of the precipitates

2. Microstructural evolution during heating

Al_xFeNi was found to be separated out steadily in the heating process. The higher the temperature reached, the larger was the aluminide particles. The formation of Al_xFeNi was not only just through the growth of originally-present particles in the as-melt spun matrix, but also through the precipitation of new particles. At the chilling sides of the ribbons, Al_xFeNi was observed to be separated out uniformly in the interior of grains where no precipitates were present originally. The microstructure of the 20 $m \cdot s^{-1}$ ribbon quenched from 520 ℃ is shown in Fig. 5a and b. The structure of the 40 $m \cdot s^{-1}$ ribbon and that of the 20 $m \cdot s^{-1}$ ribbon were very similar. Al_xFeNi precipitated along the grain boundaries could impede the coarsening of aluminium grains. Therefore, the grains were relatively smaller where more Al_xFeNi was present along the grain boundaries, and were relatively thicker where less Al_xFeNi was present along the grain boundaries.

Continuous precipitation of Al_xFeNi made its volume fraction in the ribbons significantly higher than that in the untreated commercial alloy.

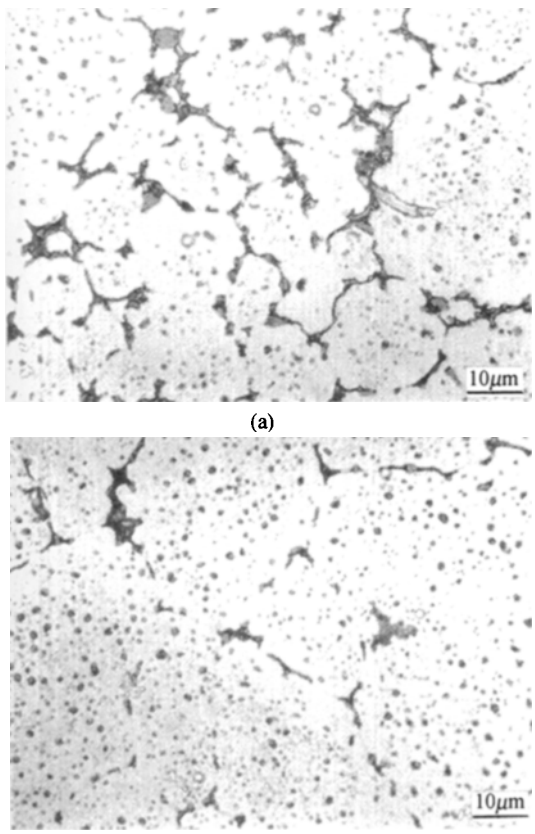

Fig. 5 Microstructure of the 20 $m \cdot s^{-1}$ ribbon after continuous heating and quenching:
(a) grains were relatively smaller if more Al_xFeNi precipitated at grain boundaries;
(b) grains were coarser if less Al_xFeNi precipitated at grain boundaries

Al_xFeNi was not found to coalescence until it melted in the matrix. DSC traces of 20 and 40 m $\cdot s^{-1}$ ribbons, B and C, are shown in Fig. 6 for comparison with that of trace A of the untreated alloy. Fig. 6 shows that the aluminide could not dissolve in the matrix on heating, but melted with the surrounding Al-matrix at certain temperature. There were small endothermic peaks in traces of both ribbons, as labeled 1 and 2 in the figure. The onset temperature of the peaks was approximately 545.3 ℃. EDX microanalyses combined with microstructural observation of ribbons quenched from 553 ℃ showed that peaks 1 and 2 were due to the eutectic melting of Al_xFeNi with the contacting aluminum. Since the content of Al_xFeNi was low in the untreated alloy, the peak of Al_xFeNi melting in trace A was very small.

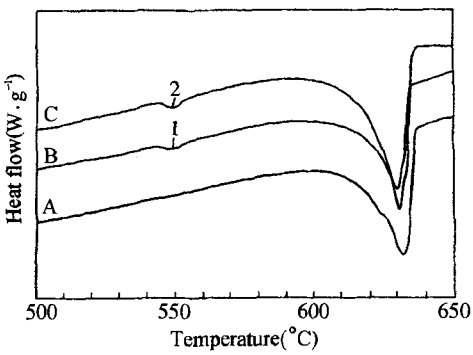

Fig.6 DSC traces of the 20 and 40 m·s^{-1} ribbons in comparison with that of untreated alloy: A- the untreated AA2618, B-the 20 m·s^{-1} ribbon, and C-the 40 m·s^{-1} ribbon

3. Effect of precipitation on the microhardness

The microhardness curve, measured at the transverse cross-section of the as-melt spun 20 m·s^{-1} ribbon, is shown in Fig.7 vs the distance from the chilling surface. It can be seen that the microhardness decreased drastically from the chilling surface to the free surface, indicating that higher cooling rate led to greater hardness.

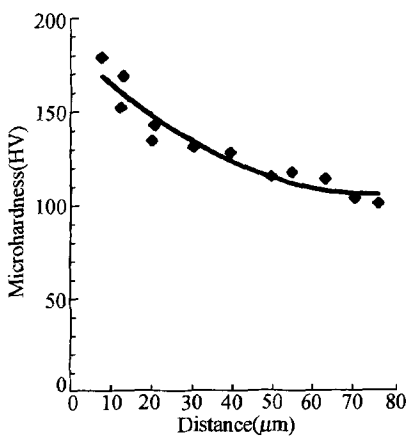

Fig.7 Curve of microhardness vs. the distance from the chilling surfaces at the transverse cross-sections of the 20 m·s^{-1} ribbon

However, the microhardness of the ribbons was not much higher compared with that of the untreated AA2618 alloy, as shown in Fig.8. The microhardness of the untreated alloy was measured as HV 160.5, and lower than the average microhardness measured on the chilling surface of the 40 m·s^{-1} ribbon (HV 184.7), but higher than the average microhardness measured on the chilling surface of the 20 m·s^{-1} ribbon (HV 152.3). After heating, along with the precipitation of alloying elements and coarsening of grains, the microhardness steadily decreased. The microhardness of the 40 m·s^{-1} ribbon was measured to be HV 146.4 when quenched from 200 ℃, HV119.14 when quenched from 535 ℃, and HV 107.52 when quenched from 553 ℃.

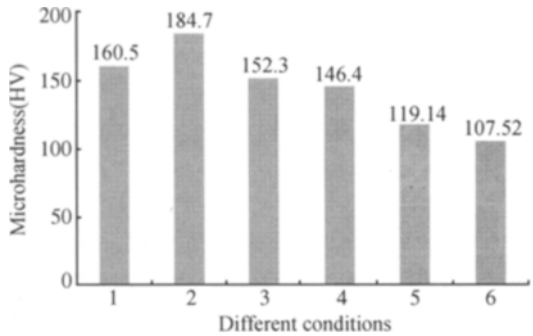

Fig.8 Comparison of microhardness under different conditions. 1. the untreated alloy; 2. on the chilling surface of as melt-spun 40 m·s^{-1} ribbon; 3. on the chilling surface of as melt-spun 20 m·s^{-1} ribbon; 4. the 40 m·s^{-1} ribbon heated to 200 ℃ then quenched; 5. the 40 m·s^{-1} ribbon heated to 535 ℃ then quenched; and 6. the 40 m·s^{-1} ribbon heated to 553 ℃ then quenched

DISCUSSION

Rapid solidification processing produces many desirable microstructural features, including extended solubility, reduced segregation, grain refinement, and formation of metastable phases. The cooling rates of melt spinning can be as high as $10^5 - 10^7$ ℃·s^{-1} (Cantor, 1994). However, at the chilling side of the 40 m·s^{-1} ribbon, where the cooling rate was the highest, there were still Al_xFeNi particles along the grain boundaries (see Fig.3b). It indicated Al_xFeNi is very prone to precipitate.

From the Al-Fe and Al-Ni binary phase diagrams, it can be found that the solubility of iron and nickel in aluminum at room temperature, or even at elevated temperatures were all close to zero, but the solubility of magnesium and copper was relatively high (see Table 2). This explains why Al_2CuMg did not precipitate on melt spinning but Al_xFeNi precipitated. Solute elements

were entrapped in the matrix during solidification due to the high cooling rate. It made the chilling sides matrix of ribbons free of precipitates. In the subsequent cooling, Al_xFeNi precipitated at the grain boundaries of the chilling sides of ribbons due to the minimal solubility of iron and nickel. The cooling was approximately Newtonian over a small solidification temperature range, and the cooling rate was proportional to the rotating speed (Cantor, 1994). Thus, the local cooling rate at the chilling surface of 20 $m \cdot s^{-1}$ ribbon was approximately half of that at the chilling surface of the 40 $m \cdot s^{-1}$ ribbon, and solute microsegregation occurred to a higher extent compared with that at the chilling side of the 40 $m \cdot s^{-1}$ ribbon. It led to the increase of Al_xFeNi precipitates at the grain boundaries of the chilling side of 20 $m \cdot s^{-1}$ ribbon.

Table 2 Solubility of elements in aluminium (Willey, L. A., 1973)

Temperature(℃)	Mg(%)	Cu(%)	Fe(%)	Ni(%)
300	3.2	0.5	≈0	≈0
100	1.0	0.1	≈0	≈0

The highest solidification rates at the chilling sides of ribbons led to a refined nondendritic structure. Away from the chilling surfaces, the grain size increased due to the decline of cooling rates (Rieker et al., 1991; Hunt, 1984). The relatively coarser structure observed at the free sides was formed through heterogeneous nucleation. The decrease of cooling rates resulted in the instability of the solidification front, and resulted in the cellular structure form (Fig. 3c, d). When the cellular growth was radical, rosette or flower structure was formed (Fig. 3d) (Willey, L. A., 1973). Moreover, due to the decrease of cooling rates the supersaturated matrix was less resistant to precipitation, and the coarsened grains lengthened the distance for solute elements to diffuse to grain boundaries. As a result, Al_xFeNi precipitation also occurred in the interior of the grains at the free sides, as seen in Fig. 3c.

Microhardness measurements of as-melt spun ribbons indicated that iron and nickel, when primarily dissolved in aluminum, could effectively strengthen the AA2618 alloy. Depending on the local cooling rates, the microhardness of the supersaturated matrix could be comparable to, or be even higher than the commercial AA2618 alloy subjected to ageing treatment (Figs. 7 and 8). The higher the cooling rate, the higher was the ribbon microhardness. In addition to solution strengthening, grain refinement was also partly responsible for the great hardness of the as-melt spun ribbons.

In the continuous heating process, the formation of GP zones and Al_2CuMg phase were restrained. Although they might form to some extent within the ageing temperature range, the precipitation amount was limited since the period of time when the Al_2CuMg stayed in the range was short, and it would be dissolved rapidly when the temperature was above the range. Thus, the effect of ageing on the hardness could be neglected. The variation of hardness primarily resulted from the precipitation of Al_xFeNi, superposed by the coarsening of aluminum grains. The result of microhardness measurements indicated that the massive precipitation led to the continuous decline of hardness; thus the steady precipitation of Al_xFeNi could lower the strength of AA2618 alloy at elevated temperatures. It suggested that further additions of iron and nickel in Al-Cu-Mg-Fe-Ni alloy might further strengthen the alloy to some extent, but the applications at high temperatures are still limited.

CONCLUSIONS

1. Al_xFeNi is very prone to precipitate in AA2618 alloy due to the minimal solubility of iron and nickel. For the AA2618 ribbons melt-spun at speeds of 20 and 40 $m \cdot s^{-1}$, refined Al_xFeNi particles could occur at the grain boundaries of the chilling sides, and could precipitate both at the grain boundaries and in the interior of grains at the free sides.

2. Al_xFeNi precipitated steadily on continuous heating. The starting temperature of Al_xFeNi melting with the surrounding Al-matrix was about 545.3 ℃.

3. The microhardnesses of as-melt spun ribbons decreased significantly from the chilling surfaces to free surfaces. The precipitation of Al_xFeNi lowered the microhardness of AA2618 alloy.

References

Birol, Y., 1996. Microstructural characterization of a rapidly-solidified Al-12wt% Si alloy. *J. Mater. Sci.*, **31**: 2139.

Cantor, B., 1994. Development of microstructure in advanced solidification processing. *Micron*. **25**: 551.

Chen, S. L., Zuo, Y., Liang, H. et al., 1997. A thermodynamic description for the ternary Al-Mg-Cu system. *Metall. Mater. Trans., A*. **28A**: 435.

Gomes, R. M., Satō, T., Tezuka, H. et al., 1996. Precipitation strengthening and mechanical properties of hypereutectic P/M Al-Si-Cu-Mg alloys containing Fe and Ni. *Mater. Sci. Forum*. **217 – 222**: 789.

Huang, C.C., and Chen, S.W., 1995. Phase equilibria of Al-rich Al-Cu-Mg alloys. *Metall. Mater. Trans., A*. **26A**: 1007.

Hunt, J. D., 1984. Steady state columar and equiaxed growth of dendrites and entectic. *Mater. Sci. Eng.*, **65**: 75.

Jones, H., 1969. Observation on a structural transition in aluminum alloy hardened by rapid solidification. *Mater. Sci. Eng.*, **5**: 1.

Oguocha, I. N. A., Yannacopoulos, S., 1996a. Natural ageing behaviour of cast alumina particle-reinforced 2618 aluminium alloy. *J. Mater. Sci.*, **31**: 3145.

Oguocha, I. N. A., Yannacopoulos, S., and Jin, Y., 1996b. The structure of Al_xFeNi phase in Al-Cu-Mg-Fe-Ni alloy (AA2618). *J. Mater. Sci.*, **31**: 5615.

Rieker, C. and Morris, D.G., 1991. Equaixed microstructure by rapid solidification. *Mater. Sci. Eng.*, **A133**: 854.

Shih, H. C., Ho, N. J., and Huang, J.C., 1996. Precipitation behaviors in Al-Mg-Cu and 2024 aluminum alloy. *Metall. Mater. Trans., A*. **27A**: 2479.

Willey, L. A., 1973. Metals Handbook, Metallography, Structures and Phase Diagrams, 8th edition, ASM, Metal Park, OH, **8**: 386.

Yao, J. Y., Geoffrey A. E. and Daniel A. G. et al., 1996. Precipitation and age-hardening in Al-Si-Cu-Mg-Fe casting alloys. *Mater. Sci. Forum*, **217 – 222**: 777.

Zhang, D. L., and Cantor, B., 1991. Heterogeneous nucleation of solidification of Si by solid Al in hypoeutectic Al-Si alloy. *In*: Proceedings of the 2nd European Conference on Advanced Materials and Processes, edited by Cline T.W. and Withers P. J., London, p.197.

Zhou, J., Duszczyk J., Korevaar, B. M., 1991. Structural development during the extrusion of rapidly solidified Al-20Si-5Fe – 3Cu – 1Mg alloy. *J. Mater. Sci.*, **26**: 824.